Ultra-high Resolution Photon Counting Detector Computed Tomography Imaging for Quantitative Lung Assessment

An Anthropomorphic Phantom Study

Jessica C. Sieren, PhD, Kimberly E. Schroeder, BSE, Jacob Kitzmann, BSE, Kevin Knoernschild, MS, Jarron Atha, BS, Natally Alarab, MD, MSc, Junfeng Guo, PhD, Sean B. Fain, PhD, and Eric A. Hoffman, PhD

Background: Quantitative lung imaging is utilized to understand, characterize, and monitor lung disease and response to interventions. X-ray computed tomography has remained the modality of choice for clinical lung assessment, and photon counting detector-computed tomography (PCD-CT) is the latest advancement. PCD-CT provides increased spatial and contrast resolution, decreased image noise and artifacts (such as beam hardening) and, thus, a potential for enhanced image quality for equivalent or reduced radiation dose levels. However, evaluation of the ultra-high resolution capabilities of PCD-CT for quantitative lung imaging has not yet been systematically investigated.

Purpose: This study aims to evaluate 2 ultra-high resolution acquisition modes and 4 reconstruction kernels for optimal quantitative chest imaging at high radiation dose (9 mGy). We assess the stability of measurements across different scan modes and reconstruction kernels when the radiation dose level is reduced.

Methods: A customized anthropomorphic chest phantom, containing standardized insert materials, including air, water, various density foam inserts, and a modulation transfer function (MTF) cube, was repeatedly scanned with PCD-CT (NAEOTOM Alpha; Siemens Healthineers). Two ultra-high resolution acquisition modes, quantum plus (UHRQ+) and quantum with tin filtering (UHRQSn), and 4 reconstruction kernels (Br64, Bl60, Qr60, and Qr40, all with iterative reconstruction level 3) were examined with acquisitions at 3 radiation dose levels (9.1 mGy, 6.8 mGy, and 3.2 mGy). Quantitative density measures, airway measurements, contrast-to-noise ratio (CNR), signal-to-noise ratio (SNR), and MTF values were compared, along with the percentage change in measurement values from high to low radiation dose levels.

Results: At the highest radiation dose levels, UHRQ+ acquisition resulted in lower density values with higher SD compared with UHRQSn. UHRQ+ mode demonstrated higher CNR, SNR, and MTF values. Only UHRQ+ with Qr40 reconstruction provided accurate air measurements, both inside and outside the phantom, across all radiation dose levels. Quantitative density measurements remained highly stable ($<2\%$ change) as the radiation dose was reduced from 9.1 to 3.2 mGy. Airway wall thickness, diameter, and lumen area measurements were all larger with UHRQ+ acquisition compared with UHRQSn for the high radiation dose level. At low radiation dose levels, the UHRQ+ acquisition with Br64 reconstruction maintained the highest consistency in airway metrics compared with the values from the high dose acquisition, with $<5\%$ measurement percentage change.

Conclusion: The UHRQ+ mode is recommended for quantitative lung assessment, leveraging the PCD-CT voxel size potential (1024×1024 in plane matrix with 0.2 mm slice thickness). The choice of reconstruction kernel at ultra-high resolution should be task-specific, with Qr40 being optimal for density assessment due to its accuracy in air measurement across regions and Br64 for airway assessment. The high consistency of measurements across the radiation dose levels for these kernels ($<5\%$ measurement change from 9 mGy measurements) suggests that acquisition at 3 mGy is sufficient for quantitative analysis.

Key Words: chest, pulmonary, lung density measures, quantitative CT, airway lumen, airway wall thickness, lung disease, protocol development

(*Invest Radiol* 2026;61:288–296)

Over the past 40 years, quantitative, volumetric x-ray CT has evolved, offering an increased understandings of lung disease etiology and progression.[1] Measurements are affected by the lung inflation state, altered voxel sizes influenced by reconstructed field of view, reconstruction kernel, artifacts such as beam hardening and image noise from the digital conversion required to capture the signal residing on energy-integrating detectors. The recent advent of ultra-high-resolution photon-counting detector (PCD) technology has the potential to significantly improve quantitative computed tomography (CT) assessment of lung anatomy and regional indices of lung function. PCD-CT offers enhanced contrast-to-noise ratios, superior spatial resolution, reduced scanning artifacts, and better structural visualization, at equivalent or reduced radiation exposure compared with energy-integrating detector (EID) technology.[2]

The key innovation of PCD technology is the direct transformation of x-ray photons into electrical signals in the semiconductor, bypassing the 2-step process of EIDs.[3,4] In EID systems, x-rays are converted to visible light within the scintillation crystal and then to electrical signal by a photodiode. PCDs eliminate the need for septa between detector pixels to minimize crosstalk, thereby enabling smaller pixel sizes and greater dose efficiency. Furthermore, PCD-CT's capability to measure the energy level of detected x-ray photons, coupled with

Received for publication April 15, 2025; and accepted for publication, after revision, June 24, 2025.

From the Department of Radiology, University of Iowa, Iowa, IA (J.C.S., K. E.S., J.K., K.K., J.A., N.A., J.G., S.B.F., E.A.H.); Department of Biomedical Engineering, University of Iowa, Iowa, IA (J.C.S., J.K., K.K.,J. G., S.B.F., E.A.H.); and Department of Internal Medicine, University of Iowa, Iowa, IA (E.A.H.).

Conflicts of interest and sources of funding: This study is supported, in part, through NIH S10 OD018526, NIH S10 OD034285 and an internal pilot grant. E.A.H. is a founder and shareholder of VIDA Diagnostics, a commercial lung image software company. J.C.S. has stock options and spousal compensation and J.G. is a shareholder of VIDA Diagnostics. The VIDA Diagnostics software was not utilized in this study. E.A.H. is an unremunerated member of the Siemens Healthineers' photon counting CT advisory board. S.B.F. reports relationships with Siemens Healthcare, GE Healthcare, Polarean, Inc., and Regeneron Pharmaceuticals Inc. that include consulting, funded grants, and travel reimbursement.

Correspondence to: Jessica C. Sieren, PhD, University of Iowa Health Care, 200 Hawkins Drive, c751GH, Iowa, IA 52242. E-mail: jessica-sieren@uiowa.edu.

Supplemental Digital Content is available for this article. Direct URL citations are provided in the HTML and PDF versions of this article on the journal's website, www.investigativeradiology.com.

ISSN: 1536-0210/26/6104–0288
DOI: 10.1097/RLI.0000000000001227

advanced iterative reconstruction methods, facilitates improved contrast at lower x-ray energies and ultra-high resolution imaging (0.2 mm detector at 1024×1024 pixel matrix, compared with traditional 0.6 mm detector at 512×512). Ultra-high resolution acquisitions, therefore, allow for unprecedented in vivo anatomic detail in the lung.

Previous studies have compared the ultra-high resolution acquisition mode of PCD-CT (1024×1024) to EID-CT in human subjects for lung disease evaluation, using equivalent or reduced radiation doses and expert reader qualitative assessments.[5–7] These studies have demonstrated that PCD-CT provides enhanced visualization of distal bronchial divisions,[5,6] sharpness of bronchial wall,[5,6] sharpness of fissure,[5,6] linear opacities,[6] bronchiectasis,[6] honeycombing,[6] and reticulation.[7] However, findings for ground-glass opacities were mixed, with one study indicating improvement with PCD-CT[7] and another preferring EID-CT.[5] In addition, one study demonstrated that EID-CT was favored for sharpness of pulmonary vessels,[5] and interstitial abnormalities.[5] Expert reviews further discuss the potential of PDC-CT for lung assessment.[8,9]

For EID-CT, spectral shaping through tin (Sn) filtering has been a valuable option for retaining image quality while reducing radiation dose levels in chest imaging.[10–12] Tin filtering is a scan acquisition option aimed at optimizing the spectrum for dose efficiency by blocking low-energy x-rays produced by the source from reaching the patient, which optimizes image quality at the interface between soft tissue and air and improves beam hardening. We incorporate tin filtering as an acquisition mode for this study to observe if spectral shaping for PCD-CT increases the stability of quantitative metrics as the radiation dose level is reduced.

Given the advancements and potential clinical advantages of PCD-CT, it is crucial to examine and optimize acquisition and reconstruction settings for quantitative assessments of lung density and structure. To date, it has been well recognized that image noise increases with reduced voxel size if radiation dose is held constant. This study aims to evaluate the performance of ultra-high resolution PCD-CT in the context of lung imaging by utilizing an anthropomorphic phantom. We compare 2 ultra-high resolution acquisition modes (with and without tin filtered spectral shaping) at a radiation dose level comparable to a standard clinical chest CT examination (9 mGy), to determine optimal performance capacity and examine the impact on quantitative measurements as radiation dose is reduced to levels used for quantitative chest CT multi-center trials (7 to 3 mGy) and low-dose CT for lung cancer screening (3 mGy).

METHODS

Photon Counting Detector-Computed Tomography Acquisition and Reconstruction

Ultra-high resolution scans were acquired on the PCD-CT (NAEOTOM Alpha; Siemens Healthineers, Forchheim, Germany; software version VA50) using 120×0.2 mm detector configuration, 140 kVp tube voltage, dose modulation (CARE keV), and rotation time of 0.25 seconds (Table 1). Two scan modes were included, the ultra-high resolution quantum plus (UHRQ+) and the ultra-high resolution quantum with tin (UHRQSn), both had 0.2 mm slice thickness and 1024×1024 matrix size. Pitch varied for the tin (Sn) filtered images (0.35 to 1.0) to match $CTDI_{vol}$ to the non-tin filtered images, which had a consistent pitch of 1.0. Three radiation levels were targeted—clinical chest CT (~9 mGy), multicenter trial CT (~7 mGy), and low-dose CT (~3 mGy). Using quantum iterative reconstruction at strength 3 (QIR 3), 4 reconstruction kernels were obtained—2 sharp kernels (Bl60 and Br64) and 2 quantitative kernels (Qr60 and Qr40).

Phantom

To evaluate the effects of acquisition scan mode, radiation dose, and reconstruction kernel on the PCD-CT images, a PH-1 N1 LUNGMAN chest phantom (Kyoto Kagaku Co., Ltd, Japan) with an added attenuation vest was utilized (Fig. 1). The phantom contained tubes with differing types of material inserts for quantitative evaluation. A 42 mm diameter tube, placed in the right lung, included 2 water inserts, a porcine fixed lung tissue sample (lung sample A), and a modulation transfer function (MTF) cube, which was custom-built at the Medical Instruments Shop at the University of Iowa Healthcare. A 22 mm diameter tube, in the left lung, contained standardized foam inserts of varying densities from the National Institute of Standards and Technology (NIST). Abdominal air was calculated through a region of interest (ROI) within the 42 mm tube, tracheal air through an ROI in the phantom trachea, and outside air was calculated through a ROI outside of the phantom. Schematic of the phantom inserts and ROIs can be seen in Figure 1A.

Image Analysis

Image analysis was performed using the in-house developed Pulmonary Analysis Software Suite (PASS),[13] which automatically segmented the regions of interest. Analysis consisted of the average and standard deviation (SD) of Hounsfield units (HU) within the insert samples. The percentage change in quantitative measures for a given scan acquisition mode, from high dose to medium and low dose, was also calculated. Contrast-to-noise (CNR) and signal-to-noise (SNR) ratios were calculated for each scan using the following equations:

$$CNR = \frac{(NIST12mean - NIST8mean)}{SD_{outside\ air}}$$

$$SNR = \frac{|mean\ of\ parechymal\ lung\ equivalent\ foam|}{SD_{outside\ air}}$$

The 3D MTF cube was made of solid high-density polyethylene. Five of the cube's sides were used to create the edge spread and line spread functions, which were then used to produce the MTF along the *x, y*, and *z* axes.[14] The 20% and 50% of peak modulations were used to assess delineation. MTF curves were plotted using R (version 4.3.0).

Airway measurements including inner and outer diameter, wall thickness, and lumen area were also calculated through PASS. These measurements were created by placing a seed point in the center of the airway. The same airway, at approximately the same axial slice, was used for all scans. Figure 1C shows an example of the output after the seed point has been placed.

Qualitative visual comparison between scan acquisition modes, reconstruction kernels and radiation dose levels included axial and coronal views, visualization of details in the fixed lung sample A, and 3 small parenchymal holes within the phantom lung that appeared outside of the insert tubes as seen in Figure 1D.

RESULTS

Visual Inspection

At a high radiation dose (9 mGy) level, for any given reconstruction kernel, the UHRQSn acquisition featured less streaking (beam hardening) compared with the UHRQ+

TABLE 1. Acquisition and Reconstruction Parameters for Photon Counting Detector Computed Tomography (PCD-CT) Chest Phantom Scans

Parameters	UHRQ+	UHRQSn
Acquisition		
Detector configuration, # x mm	120 × 0.2	120 × 0.2
Rotation time, s	0.25	0.25
Pitch	1.0	0.35, 0.45, 1.0
Tube potential, kVp	140	Sn140
Care keV	On	On
Care keV IQ	80, 57, 26	103, 75, 36
CTDIVol, mGy	9.1, 6.8, 3.2	9.1, 6.8, 3.2
Reconstruction		
Slice thickness x spacing, mm	0.2 × 0.15	0.2 × 0.15
Matrix size	1024×1024	1024×1024
Field of view, mm	260	260
Kernels	Br64, Bl60, Qr60, Qr40	Br64, Bl60, Qr60, Qr40
Iterative reconstruction	QIR; strength 3	QIR; strength 3

acquisition in the simulated fat surrounding the ribs in the axial view (Fig. 2) and at the apex of the lungs in the coronal view (Supplemental Fig. 1, Supplemental Digital Content 1, http://links.lww.com/RLI/B47). This reduction in noise around the ribs and apex of the lung is less evident at low dose (3 mGy). At 3 mGy, the UHRQ+ acquisition provides clearer small structure definition compared with UHRQSn, as made evident by the clarity of the boundaries of the small parenchymal holes shown in Figure 2 (right inset). Visual inspection of the 4 reconstruction kernels investigated, identified Qr60 as providing a balance between low noise and edge detection (Fig. 2).

High Radiation Dose Protocol Comparison

Comparing quantitative measurements for the phantom inserts from UHRQ+ (Table 2) and UHRQSn (Table 3) scan modes for the high radiation dose protocol revealed a consistent trend in lower SDs in the UHRQSn acquisitions compared with the equivalent kernel reconstruction acquired with UHRQ+ mode. For the outside air measurement, the SD was lower in the UHRQ+ acquired data. The NIST foam insert measurements showed a consistent trend (across all reconstruction kernels) to lower mean HU density with UHRQ+ compared with UHRQSn acquisition mode. For the lowest density NIST foam insert (NIST 4 lb), which mimicked emphysematous lung parenchyma, the mean HU difference between scan modes was the greatest [UHRQ+ - UHRQSn ranged from -12.73HU (Br64) to -11.46HU (Qr60)]. These observed trends in SD, and mean HU measurements of the NIST foam persisted at the low radiation dose (Supplemental Tables 1 and 2, Supplemental Digital Content 1, http://links.lww.com/RLI/B47).

There was a systematically higher contrast-to-noise ratio (CNR) and signal-to-noise ratio (SNR) in the UHRQ+ compared with UHRQSn mode acquisitions at the high radiation dose level (9 mGy). The highest CNR (5.29) and SNR (49.66) were with the UHRQ+ acquisition mode and Qr40 reconstruction kernel. The lowest CNR (0.91) and SNR (8.84) were with the UHRQSn acquisition mode and Bl60 kernel.

The spatial frequency cutoffs for the modulation transfer function (MTF) were slightly higher for the UHRQ+ versus UHRQSn acquisition mode for the Br64, Qr60, and Qr40 reconstruction kernels, respectively (refer to Supplemental Fig. 2, Supplemental Digital Content 1, http://links.lww.com/RLI/B47 for the MTF curves). The highest spatial frequency cutoffs for the MTF were achieved with the Bl60 reconstruction kernel, for which the 50% modulation cutoff was 8.59 cycles/cm in-plane and 10.07 cycles/cm in the z-direction (Table 2). As expected, the Qr40 kernel, being the softest kernel included in the evaluation, had the lowest spatial frequency cutoff for the MTF, with the 50% modulation cutoff being 3.37 cycles/cm in-plane and 7.49 cycles/cm in the z-direction.

Comparison to Reference Values for Water and Air Measurements

Table 4 illustrates the reference value minus the measurement value for air and water regions of interest within the phantom. For quantitative measurement of water (water 1 and water 2) in the anthropomorphic chest phantom, measurements

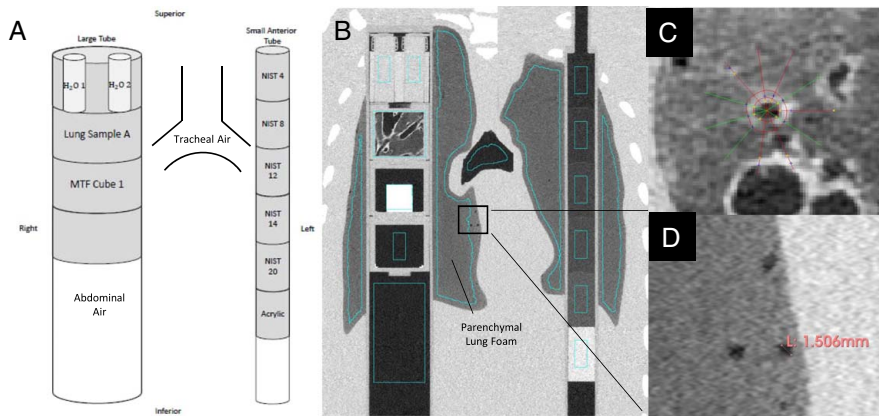

FIGURE 1. Anthropomorphic chest phantom with inserts for quantitative measurement evaluation. A, Phantom insert configuration including right lung large tube (42 mm) with water (H_2O) inserts, fixed lung sample A, modulation transfer function (MTF) cube, and abdominal air region. Air measurements were also assessed in the trachea of the phantom and outside the phantom (not illustrated in the schematic). Left lung small tube includes varying density foam inserts from the National Institute of Standards and Technology (NIST; acrylic insert not analyzed). B, Compilation of coronal slices showing the automated segmentations (blue outlines) of the inserts, including the parenchymal lung foam region. C, Example of the automated airway measurement made in the axial plane of lung sample A. D, Zoomed in example of the 3 parenchymal holes measuring ~1.5 mm.

Copyright © 2025 Wolters Kluwer Health, Inc. All rights reserved.

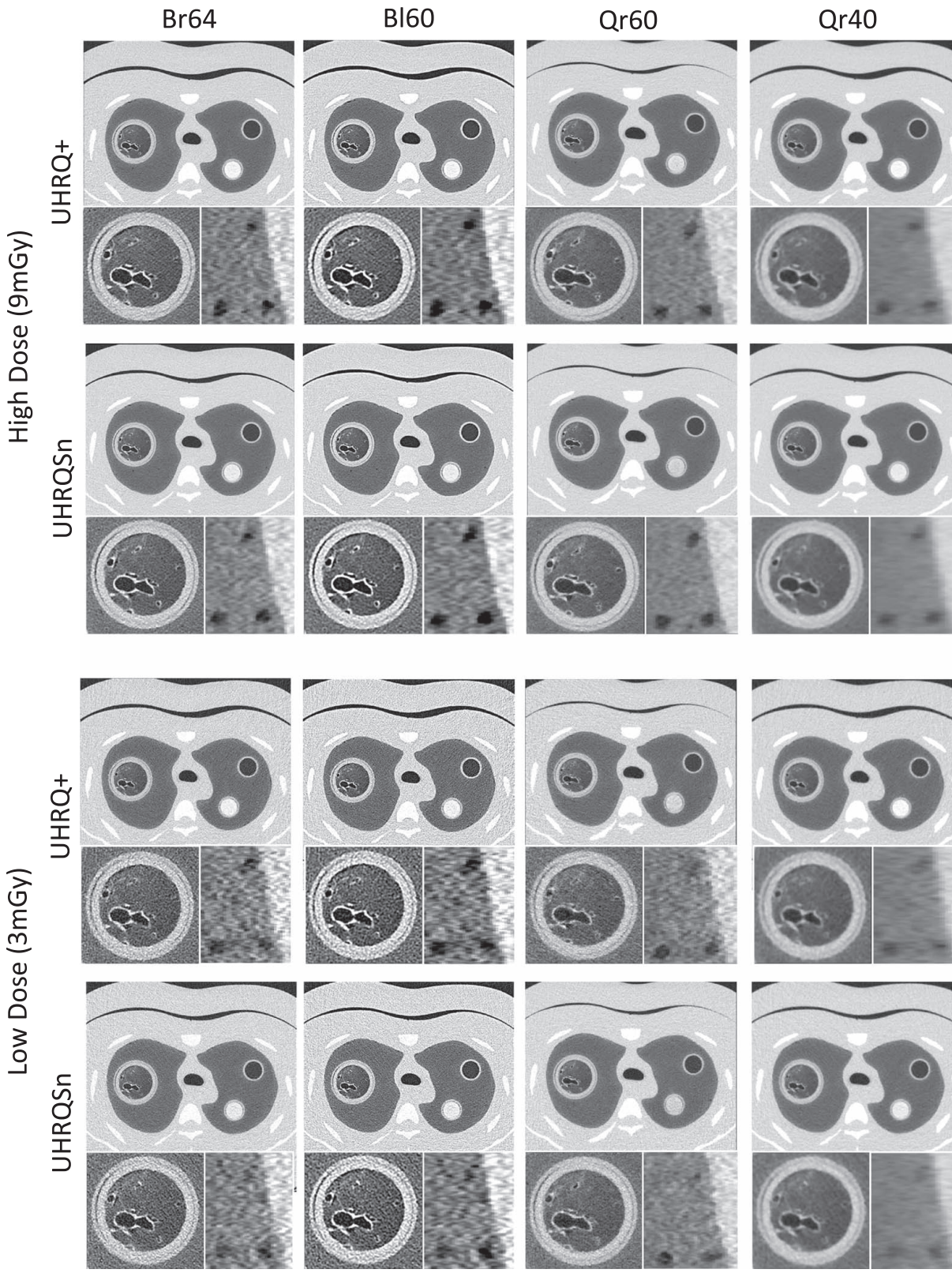

FIGURE 2. Representative images for photon counting protocol comparison across 2 radiation dose levels (9 mGy and 3 mGy), 2 scan acquisition modes (HRUQ+ and UHRQSn), and 4 reconstruction kernels (Br64, Bl60, Qr60, and Qr40). Axial cross-section of phantom at the level of lung sample A, NIST-8 and bone 50% (not analyzed). Inset imaging show the lung sample A, which is contained in a tube of 42 mm diameter (left inset) and 3 parenchymal holes of ~1.5 mm each (right inset).

TABLE 2. Quantitative Measurements for Photon Counting Detector Computed Tomography (PCD-CT) Phantom Acquisition With High Radiation Dose (9 mGy) and UHRQ+ Acquisition Mode (No Tin Filtering)

UHRQ+	Mean (SD)			
HU	Br64	Bl60	Qr60	Qr40
Abdominal air	−1023.99 (106.57)	−1023.96 (118.66)	−1015.10 (65.53)	−1004.16 (24.85)
Tracheal air	−1006.06 (95.75)	−1017.23 (106.95)	−999.89 (59.37)	−990.93 (25.23)
Outside air	−1012.17 (56.21)	−1012.92 (63.62)	−1004.34 (35.83)	−1000.43 (12.76)
Water vial 1	−0.74 (119.43)	0.05 (136.33)	0.62 (73.30)	−1.12 (28.75)
Water vial 2	−1.28 (113.39)	−0.30 (127.88)	−2.62 (70.49)	−1.79 (28.75)
Lung sample A	−630.09 (289.65)	−648.86 (363.19)	−614.10 (248.77)	−601.93 (221.94)
Foam inserts				
NIST 4 lb	−955.62 (98.67)	−957.84 (111.23)	−950.70 (60.03)	−942.50 (23.47)
NIST 8 lb	−902.42 (92.41)	−903.10 (103.36)	−896.02 (57.26)	−889.50 (21.29)
NIST 12 lb	−834.73 (88.91)	−835.39 (99.50)	−828.11 (55.57)	−822.00 (20.10)
NIST 14 lb	−791.24 (90.99)	−791.56 (101.75)	−784.34 (55.83)	−779.92 (20.56)
NIST 20 lb	−694.30 (110.05)	−694.86 (123.12)	−687.84 (67.13)	−686.52 (25.07)
Ratios				
CNR	1.20	1.06	1.90	5.29
SNR	11.36	10.6	17.71	49.66
MTF cycles/cm				
CF50%, in plane	8.34	8.56	6.19	3.47
CF20%, in plane	11.35	12.51	9.47	5.21
CF50%, Z-plane	7.80	9.93	7.67	7.74
CF20%, Z-plane	14.73	17.42	14.29	14.52

were within ±4 HU of the reference value (0 HU) for all radiation dose levels, scan modes and reconstruction kernels.

For air measurements, only the UHRQ+ acquisition mode with the Qr40 reconstruction kernel was within ±10 HU of the air reference standard (-1000 HU) for all 3 radiation dose levels, and across all 3 air ROIs (outside, tracheal, and abdominal). For the UHRQSn acquisition mode, at the high radiation dose level, the outside air measurements were within ±10 HU across all 4 reconstruction kernels. The differences from reference standard for the Qr60 and Qr40 kernels remained within ±10 HU as dose decreased for outside air and abdominal air measurements but were >10 HU for tracheal air (Table 4).

Airway Assessment

The airway measurements were made using the fixed airway in the lung sample A insert (Fig. 1C), hence, there is no reference standard to which measurement values can be compared; however, measures were generally consistent with the relative performance based on the MTF. In general, the UHRQ+ acquisition mode resulted in slightly larger airway-associated metrics (lumen area, inner diameter, outer diameter, and wall thickness) compared with UHRQSn for the equivalent reconstruction kernel (Table 5). In the Qr40 reconstructions, across both acquisition modes and all radiation doses, there was larger outer diameter (ranging from

TABLE 3. Quantitative Measurements for Photon Counting Detector Computed Tomography (PCD-CT) Phantom Acquisition With High Radiation Dose (9 mGy) and UHRQSn Acquisition Mode (Includes Tin Filtering)

UHRQSn	Mean (SD)			
HU	Br64	Bl60	Qr60	Qr40
Abdominal air	−1010.54 (86.55)	−1011.72 (96.42)	−1002.13 (53.40)	−992.86 (20.87)
Tracheal air	−991.20 (85.61)	−1002.52 (95.58)	−984.89 (52.85)	−977.02 (23.46)
Outside air	−1009.64 (62.79)	−1009.53 (71.22)	−1000.68 (38.79)	−995.94 (14.43)
Water vial 1	−0.49 (101.78)	−0.35 (115.97)	−1.56 (62.35)	−0.89 (25.09)
Water vial 2	−3.17 (98.42)	−2.85 (111.28)	−1.88 (61.06)	−3.58 (24.74)
Lung sample A	−617.77 (278.49)	−636.68 (348.96)	−603.61 (242.63)	−592.68 (219.34)
Foam inserts				
NIST 4 lb	−942.90 (87.14)	−945.40 (98.06)	−939.24 (53.89)	−930.64 (21.09)
NIST 8 lb	−892.88 (80.15)	−894.36 (90.39)	−887.11 (48.84)	−880.72 (18.83)
NIST 12 lb	−827.70 (76.05)	−829.41 (85.23)	−821.20 (46.13)	−816.65 (17.07)
NIST 14 lb	−784.17 (78.31)	−785.88 (87.78)	−777.68 (47.80)	−774.76 (17.77)
NIST 20 lb	−685.63 (87.26)	−687.65 (97.73)	−680.73 (53.79)	−680.09 (20.32)
Ratios				
CNR	1.04	0.91	1.70	4.44
SNR	9.99	8.84	16.12	43.31
MTF cycles/cm				
CF50%, in plane	8.23	8.59	5.74	3.37
CF20%, in plane	11.09	12.56	9.07	5.11
CF50%, Z-plane	7.48	10.07	7.53	7.49
CF20%, Z-plane	13.80	16.80	13.40	13.81

TABLE 4. The Difference Between Reference Values for air (–1000 HU) and water (0 HU) and the Measured Hounsfield Unit Values From the Anthropomorphic Phantom Across 2 Scan Acquisition Modes (UHRQ+ and UHRQSn), 3 Radiation Dose Levels (High, Medium, Low), and 4 Reconstruction Kernels (Br64, Bl60, Qr60, and Qr40)

			Difference From Reference Values (HU)				
Scan Mode	**Dose Level**	**Recon Kernel**	**Tracheal Air**	**Abdominal Air**	**Outside Air**	**Water 1**	**Water 2**
UHRQ+	High	Br64	6.06	23.99*	12.17*	0.74	1.28
UHRQ+	High	Bl60	17.23*	23.96*	12.92*	−0.05	0.30
UHRQ+	High	Qr60	−0.11	15.10*	4.34	−0.62	2.62
UHRQ+	High	Qr40	−9.07	4.16	0.43	1.12	1.79
UHRQ+	Medium	Br64	7.52	25.73*	16.80*	−0.48	1.86
UHRQ+	Medium	Bl60	18.22*	24.63*	15.54*	−1.09	0.80
UHRQ+	Medium	Qr60	0.87	16.74*	5.81	0.38	1.00
UHRQ+	Medium	Qr40	−8.33	4.56	0.62	0.21	2.43
UHRQ+	Low	Br64	18.65*	27.42*	19.39*	−0.72	1.22
UHRQ+	Low	Bl60	17.78*	24.61*	16.75*	−1.72	−0.07
UHRQ+	Low	Qr60	1.39	18.14*	12.19*	1.58	2.94
UHRQ+	Low	Qr40	−8.23	4.97	0.37	0.54	1.84
UHRQSn	High	Br64	−8.80	10.54*	9.64	0.49	3.17
UHRQSn	High	Bl60	2.52	11.72*	9.53	0.35	2.85
UHRQSn	High	Qr60	−15.11*	2.13	0.68	1.56	1.88
UHRQSn	High	Qr40	−22.98*	−7.14	−4.06	0.89	3.58
UHRQSn	Medium	Br64	−7.07	12.34*	10.59*	1.22	2.24
UHRQSn	Medium	Bl60	3.54	12.38*	10.22*	0.99	1.96
UHRQSn	Medium	Qr60	−14.12*	3.77	2.19	0.71	2.70
UHRQSn	Medium	Qr40	−22.53*	−7.13	−3.93	1.47	2.90
UHRQSn	Low	Br64	13.84*	16.25*	17.72*	−1.56	1.12
UHRQSn	Low	Bl60	11.54*	13.80*	13.55*	−2.59	0.14
UHRQSn	Low	Qr60	−8.78	7.54	6.50	0.15	1.23
UHRQSn	Low	Qr40	−20.57*	−5.72	−3.71	0.42	2.37

All measured water values were within ± 4 HU of the reference value. Measured air values differences more than ± 10 HU from the reference value are highlighted with an asterisk (*).

TABLE 5. Airway Measurements for a Target Airway in the Phantom's fixed Lung Sample A Insert Across 2 Scan Acquisition Modes (UHRQ+ and UHRQSn), 3 Radiation Dose Levels (High, Medium, Low), and 4 Reconstruction Kernels (Br64, Bl60, Qr60, and Qr40)

			Mean (SD)			Lumen Area (mm^2)
Scan Mode	**Dose Level**	**Recon Kernel**	**Inner Diameter (mm)**	**Outer Diameter (mm)**	**Wall Thickness (mm)**	**Mean**
UHRQ+	High	Br64	2.63 (0.23)	4.40 (0.15)	0.89 (0.11)	5.39
UHRQ+	High	Bl60	2.55 (0.28)	4.36 (0.18)	0.91 (0.09)	5.01
UHRQ+	High	Qr60	2.56 (0.29)	4.29 (0.34)	0.87 (0.20)	4.94
UHRQ+	High	Qr40	2.37 (0.23)	5.04 (0.35)	1.34 (0.18)	4.34
UHRQ+	Medium	Br64	2.57 (0.28)	4.53 (0.34)	0.98 (0.14)	5.20
UHRQ+	Medium	Bl60	2.46 (0.19)	4.59 (0.42)	1.07 (0.19)	4.76
UHRQ+	Medium	Qr60	2.62 (0.29)	4.38 (0.67)	0.88 (0.25)	5.32
UHRQ+	Medium	Qr40	2.31 (0.14)	5.28 (0.51)	1.49 (0.25)	4.18
UHRQ+	Low	Br64	2.65 (0.37)	4.41 (0.30)	0.88 (0.21)	5.59
UHRQ+	Low	Bl60	2.58 (0.33)	4.51 (0.24)	0.97 (0.12)	5.27
UHRQ+	Low	Qr60	2.71 (0.27)	4.22 (0.39)	0.76 (0.11)	5.98
UHRQ+	Low	Qr40	2.46 (0.26)	5.23 (0.35)	1.38 (0.16)	4.77
UHRQSn	High	Br64	2.50 (0.25)	4.15 (0.17)	0.83 (0.08)	4.94
UHRQSn	High	Bl60	2.35 (0.26)	4.12 (0.21)	0.89 (0.06)	4.40
UHRQSn	High	Qr60	2.46 (0.31)	4.07 (0.27)	0.80 (0.13)	4.67
UHRQSn	High	Qr40	2.33 (0.23)	5.10 (0.81)	1.38 (0.36)	4.34
UHRQSn	Medium	Br64	2.64 (0.24)	4.64 (0.53)	1.00 (0.27)	5.37
UHRQSn	Medium	Bl60	2.44 (0.22)	4.54 (0.44)	1.05 (0.29)	4.62
UHRQSn	Medium	Qr60	2.69 (0.21)	4.06 (0.31)	0.69 (0.07)	5.46
UHRQSn	Medium	Qr40	2.34 (0.12)	5.04 (0.65)	1.35 (0.33)	4.26
UHRQSn	Low	Br64	2.68 (0.34)	4.20 (0.32)	0.76 (0.25)	5.61
UHRQSn	Low	Bl60	2.62 (0.28)	4.34 (0.23)	0.86 (0.14)	5.14
UHRQSn	Low	Qr60	2.27 (0.36)	4.02 (0.38)	0.88 (0.17)	3.94
UHRQSn	Low	Qr40	2.40 (0.18)	5.33 (0.42)	1.47 (0.27)	4.51

Measurements from the Qr40 reconstructed scans have larger outer diameter and wall thickness measurements compared with the measures from other reconstruction kernels.

5.04 ± 0.65 to 5.33 ± 0.42 mm) and wall thickness measurements (ranging from 1.33 ± 0.18 to 1.49 ± 0.25 mm), while all other reconstruction kernels (Br64, Bl60, and Qr60) produced measurements in alignment with each other (outer diameter measurement range from 4.02 ± 0.38 to 4.64 ± 0.53 mm and wall thickness measurement range from 0.76 ± 0.11 to 1.07 ± 0.19 mm).

Stability of Quantitative Measurements as Radiation Dose Level Is Reduced

To compare the measurement stability across scan modes (UHRQ+ and HURQSn) and reconstruction kernel (Br64, Bl60, Qr60, and Qr40) as the radiation dose level was decreased, the percentage measurement change was calculated. Figure 3 tabulates the quantitative percentage measurement change from high dose to low dose (high dose to medium dose data is shown in Supplemental Fig. 3, Supplemental Digital Content 1, http://links.lww.com/RLI/B47). The percentage change values were low for the NIST foam inserts (0% to -0.6%) and low for regions of air (-0.02% to 1.22%), demonstrating high concordance with the measures acquired at the high radiation dose level.

The largest change impacted the CNR and SNR measurements, which decreased ~40% at low dose for UHRQSn, and ~30% for UHRQ+. Percentage measurement change was variable for the airway quantification with a tendency for larger values for airway structures at low dose (indicated by positive percentage measurement change values). Lumen area had the greatest percentage measurement change from high to low dose, across scan modes and reconstruction filters, with larger values (+3.9% to +21% change) for all but one acquisition/kernel reconstruction (UHRQSn, Qr60, -15.6% change). Wall thickness, in contrast, had variable percentage measurement change across scan modes and reconstruction kernels, ranging from -12% to +9.24%. The UHRQ+ with Br64 reconstruction had the highest consistency for airway measurements at reduced acquisition radiation dose, with percentage measurement change within ±5% for wall thickness, inner and outer diameter, and airway lumen area.

DISCUSSION

The anthropomorphic phantom allows for the careful comparison of quantitative results across multiple PCD-CT scan acquisition settings. This study has focused on the comparison of ultra-high resolution modes (with and without tin filtering) and a range of radiation dose levels. We also compared results across a range of reconstruction kernels that have been used in previous PCD-CT studies: Br64,[15] Bl60,[5,6,16] Qr60,[17] and Qr40.[2,16,18] Importantly, our results indicate that for the use of the UHRQ + mode for quantitative lung assessment, the quantitative density and airway measurements were highly stable as radiation dose was reduced from 9 to 3 mGy, with the expected measurement changes occurring in CNR, SNR and consequently in in-plane MTF.[19]

Qualitative visual inspection of the image data revealed that UHRQSn provided small improvements to images generated using the highest radiation dose levels, particularly with less beam hardening at the apex of the lung. However, at lower doses, UHRQ+ provided clearer boundary visualization of small objects. In particular, the Qr60 reconstruction kernel was found to have the best compromise for the parameter settings studied between image noise and delineation of small structures (ie, the 3 parenchymal holes illustrated in Figure 2). This was supported quantitatively by the higher CNR, SNR and MTF values for the UHRQ+ acquisition mode. As expected, the sharper kernels have the best MTF performance, while the softest kernel has the best CNR and SNR performance, thus kernel selection at high dose should depend on the task priority.

Data were reconstructed to maximize the spatial resolution possible with the ultra-high resolution scan modes, including both the expanded in-plane matrix (1024×1024) and 0.2 mm in-plane detector size and slice thickness (0.15 mm). With these setting, we found the UHRQ+ acquisition mode with Qr40 reconstruction kernel was the only acquisition mode and kernel combination that had water, outside air, abdominal air and tracheal air measurement within empirical tolerances of ±4 HU of 0 HU for water, and ±10 HU of -1000 HU for air across all 3 radiation dose levels. This deviation from -1000 HU for higher frequency kernels may be due to the combined impact of the very small slice thickness and iterative reconstruction (QIR 3). In another study, similar protocol settings, but using thicker reconstruction slice thickness (>0.5 mm) with QIR 2 and QIR 4, found air measurements in the anthropomorphic phantom did not have such pronounced deviations from -1000 HU.[20] The SD for outside air measurements was lower, compared with tracheal and abdominal air, in both the UHRQ+ and UHRQSn (but to a lesser degree) scan modes. This finding mirrors that from Malkus and Szczykutowicz[21] who reported an approximately factor of 2 decrease in SD in outside air compared with within a water phantom. Our results indicate further refinement of reconstruction algorithms may be required for quantitative assessment at ultra-high resolution with 0.2 mm slice thickness.

In this study, we did not find superior quantitative assessment concordance at low radiation dose acquisition with UHRQSn acquisition mode. This indicates that at the doses explored in this study, there is minimal improvement for beam hardening and image quality through tin filtering, beyond what is achieved through the energy discrimination from PCD-CT technology. Spectral shaping with tin filtration resulted in a trend to higher density (HU) values and smaller airway values compared with UHRQ+ mode at high radiation dose levels. Higher HU measurements with UHRQSn, especially for high-density materials, are expected due to the adjusted mean energy with spectral shaping compared with non-tin filtered and use of polychromatic reconstruction. As an aside, this is also why URHQSn mode is not recommended for contrast-enhanced CT. When looking at the percentage measurement change from high radiation dose to low radiation dose, there was no increased measurement stability at low dose with tin filtration. However, it is possible that the UHRQSn has some image quality advantages at ultra-low radiation dose levels (<3 mGy) not examined in this study. Another consideration for the comparison of the scan modes is acquisition time. The UHRQSn acquisition at highest and medium radiation dose levels had a smaller pitch (0.35 and 0.45, respectively, compared with 1.0 for other protocols), and hence slightly longer acquisition time (~10 s). For the UHRQSn mode, the scanning platform did not allow increased CARE keV IQ (which adjusts the reference mAs) to a level that matched the highest and medium dose levels, and hence, the pitch had to be adjusted to achieve matched $CTDI_{vols}$. While not evaluated in the anthropomorphic phantom, it is possible that human volunteer or patient scanned in vivo over the longer acquisition time could result in decreased image quality from cardiac motion.

This study does have some limitations. The focus was on the evaluation of quantitative measurement relevant to the lung using an anthropomorphic phantom, which has been utilized in other studies looking at quantitative lung imaging CT protocol development and comparison[22,26] However, phantom data does not capture some of

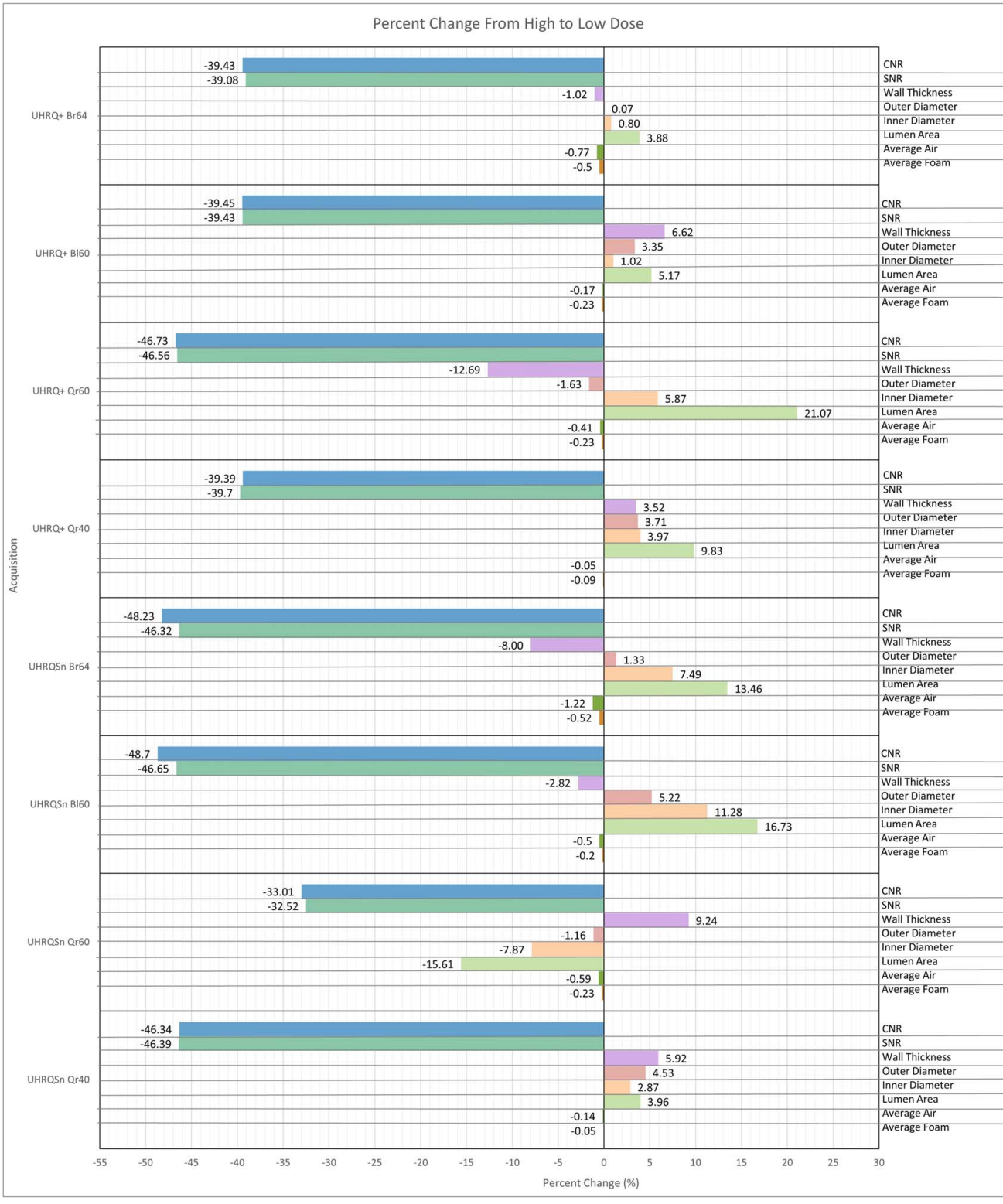

FIGURE 3. Percentage measurement change comparing the high dose (9 mGy) to the low dose (3 mGy) quantitative values.

the complexity of human subjects, such as cardiac motion and/or variations in body mass index. Future work will be a translational study to validate findings in a biological model, as we have previously performed,[11,24] before translating the protocol to quantitative lung assessment in humans. In this study, we did not explore the impact of different iterative reconstruction levels. We selected to focus on one quantum iterative reconstruction level (QIR 3) based on prior work by Sartoretti et al,[25] illustrating QIR 3 performed best for image quality and sharpness by expert readers, and other work in the literature focusing on QIR 3.[5,6,26] The reconstruction kernels selected focused on those from prior publications, future work will explore the Qr64 reconstruction kernel for airway evaluation.

Results from this study indicate the use of the UHRQ+ mode for quantitative lung assessment. With PCD-CT technology, the quantitative density and airway measurements were highly stable as radiation dose was reduced from 9 to 3 mGy, with the only substantial measurement changes occurring in CNR, SNR and consequently in-plane MTF. Ideally, 2 reconstructions would be produced for quantitative lung assessment: (1) Qr40 used for density assessment due to accuracy of air measurement across regions and high CNR and SNR, and (2) Br64 used for airway evaluation as, despite a slightly lower MTF spatial frequency cutoff than the Bl60 kernel, the Br64 kernel produced more consistent airway wall, diameter and lumen area measurements as dose was lowered from 9 to 3 mGy.

ACKNOWLEDGMENTS

The authors thank Juan Carlos Ramirez Giraldo, Andrew Primak, Matthew Fuld, and Erin Grunewald for technical assistance with the Siemens NAEOTOM Alpha system.

REFERENCES

1. Hoffman EA. Origins of and lessons from quantitative functional X-ray computed tomography of the lung. *Br J Radiol*. 2022;95:20211364.
2. Liu LP, Shapira N, Chen AA, et al. First-generation clinical dual-source photon-counting CT: ultra-low-dose quantitative spectral imaging. *Eur Radiol*. 2022;32:8579–8587.
3. Flohr T, Schmidt B. Technical basics and clinical benefits of photon-counting CT. *Invest Radiol*. 2023;58:441–450.
4. Koons EK, Thorne JE, Huber NR, et al. Quantifying lumen diameter in coronary artery stents with high-resolution photon counting detector CT and convolutional neural network denoising. *Med Phys*. 2023;50:4173–4181.
5. Milos RI, Röhrich S, Prayer F, et al. Ultrahigh-resolution photon-counting detector CT of the lungs: association of reconstruction kernel and slice thickness with image quality. *AJR Am J Roentgenol*. 2023;220:672–680.
6. Gaillandre Y, Duhamel A, Flohr T, et al. Ultra-high resolution CT imaging of interstitial lung disease: impact of photon-counting CT in 112 patients. *Eur Radiol*. 2023;33:5528–5539.
7. Inoue A, Johnson TF, White D, et al. Estimating the clinical impact of photon-counting-detector CT in diagnosing usual interstitial pneumonia. *Invest Radiol*. 2022;57:734–741.
8. McCollough CH, Rajendran K, Baffour FI, et al. Clinical applications of photon counting detector CT. *Eur Radiol*. 2023;33:5309–5320.
9. Remy-Jardin M, Hutt A, Flohr T, et al. Ultra-high-resolution photon-counting CT imaging of the chest: a new era for morphology and function. *Invest Radiol*. 2023;58:482–487.
10. Newell JD Jr, Fuld MK, Allmendinger T, et al. Very low-dose (0.15 mGy) chest CT protocols using the COPDGene 2 test object and a third-generation dual-source CT scanner with corresponding third-generation iterative reconstruction software. *Invest Radiol*. 2015;50:40–45.
11. Hammond E, Sloan C, Newell JD Jr, et al. Comparison of low- and ultralow-dose computed tomography protocols for quantitative lung and airway assessment. *Med Phys*. 2017;44:4747–4757.
12. Martini K, Higashigaito K, Barth BK, et al. Ultralow-dose CT with tin filtration for detection of solid and sub solid pulmonary nodules: a phantom study. *Br J Radiol*. 2015;88:20150389.
13. Guo J, Fuld M, Alford S, et al. Pulmonary Analysis Software Suite 9.0: Integrating quantitative measuresof function with structural analyses, Proceedingsof the FirstInternational Workshop on Pulmonary Image Processing, Iowa City, IA, 2008;1:283–292.
14. Guo J, Atha J, Halaweish A, et al. A novel device to measure 3D MTF accounting for CT scanner, protocol and the thoracic environment. *Am J Respir Crit Care Med*. 2021;203:A4595.
15. McCabe C, Sauer TJ, Zarei M, et al. A systematic assessment of photon-counting CT for bone mineraldensity and microarchitecture quantifications. *Proc SPIE Int Soc Opt Eng*. 2023;12463:1.
16. Heck L, Liu L, Pasyar P, et al. First-generation clinical dual-source photon-counting CT: quantitative and ultra-high-resolution spectral imaging. *Med Imaging 2023 Phys Med Imaging*. 2023;1246320:77.
17. Ho FC, Sotoudeh-Paima S, Segars WP, et al. Development and application of a virtual imaging trial framework for airway quantifications via CT. *Proc SPIE Int Soc Opt Eng*. 2023:50.
18. Deleu M, Maurice JB, Devos L, et al. Image quality analysis of photon-counting CT compared with dual-source CT: a phantom study for chest CT examinations. *Diagnostics*. 2023;13:1325.
19. Richard S, Husarik DB, Yadava G, et al. Towards task-based assessment of CT performance: system and object MTF across different reconstruction algorithms. *Med Phys*. 2012;39:4115–4122.
20. Alarab N, Guo J, Atha J, et al. Optimizing ChestCT With Photon-counting Detector Technology: Comparison to Established Energy-integrating Detector CT Protocols, in American Thoracic Society Meeting, San Diego, CA. *Am J Respir Crit Care Med*. 2024;209.
21. Malkus A, Szczykutowicz TP. A method to extract image noise level from patient images in CT. *Med Phys*. 2017;44:2173–2184.
22. Shankar SS, Felice N, Hoffman EA, et al. Task-based validation and application of a scanner-specific CT simulator using an anthropomorphic phantom. *Med Phys*. 2022;49:7447–7457.
23. Hammond E, Chan KS, Ames JC, et al. Impact of advanced detector technology and iterative reconstruction on low-dose quantitative assessment of lung computed tomography density in a biological lung model. *Med Phys*. 2018;45:3657–3670.
24. Sartoretti T, Racine D, Mergen V, et al. Quantum iterative reconstruction for low-dose ultra-high-resolution photon-counting detector CT of the lung. *Diagnostics*. 2022;12:522.
25. Jungblut L, Euler A, von Spiczak J, et al. Potential of photon-counting detector CT for radiation dose reduction for the assessment of interstitial lung disease in patients with systemic sclerosis. *Invest Radiol*. 2022;57:773–779.
26. Shankar SS, Hoffman EA, Atha J, et al. Inter- and intra-scan variability for lung imaging quantifications via CT. *Proc SPIE Int Soc Opt Eng*. 2022;12031.